Journal of Machine Engineering, 2018, Vol. 18, No. 3, 87–97
ISSN 1895-7595 (Print) ISSN 2391-8071 (Online)

Received: *15 January 2018* / Accepted: *09 March 2018* / Published online: *28 September 2018*

coefficient of thermal expansion,
phase transformation model,
hot stamping

Thawin HART-RAWUNG[1*]
Johannes BUHL[1]
Markus BAMBACH[1]

EXTENSION OF A PHASE TRANSFORMATION MODEL FOR PARTIAL HARDENING IN HOT STAMPING

The quality of predicted microstructural and mechanical properties in hot stamping simulations relies considerably on the material model. Many researchers studied the effect of the plastic deformation on the phase transformation of the most commonly used hot stamping steel 22MnB5, and proved that the deformation applied at high temperature promotes the formation of ferrite, pearlite and bainite. This behaviour has to be integrated into materials modelling. In this study, the effect of pre-strain on the phase transformation of the material is considered. The specimens are heated to austenitization temperature, isothermally deformed at 700°C, and quenched down to room temperature. The phase fractions and the temperature-dilatation behaviour obtained from the experiments are used to calibrate the material model. By using the experimental data obtained from dilatometer testing, the accuracy of the material model is evaluated. Additionally, an attempt to predict the results between the tested data points by using interpolation was made and compared with the simulation results.

1. INTRODUCTION

Lightweight components reduce the overall weight of a structure and are a key element for the automotive industry in achieving CO_2 emission goals according to current legislation. The continuously increasing demand for the cost optimization of lightweight components increases the need for virtual development and testing of new workpiece designs and process routes [1]. In automotive mass production, hot stamped steel components provide the best compromise between cost and lightweight performance. Presently, there are several hot stamping process routes. The direct-hot stamping process starts with the heating of the blank to austenitization temperature. Then, the material is held for a certain time in order to achieve a homogeneous austenite microstructure. Next, the material is transferred and formed in a forming die. At the end of the forming step, the material is held and quenched in the cooled forming die to obtain the desired

[1] Chair of Mechanical Design and Manufacturing, Brandenburg University of Technology Cottbus-Senftenberg, Cottbus, Germany
[*] E-mail: thawihar@b-tu.de
https://doi.org/10.5604/01.3001.0012.4619

microstructure and properties. If the cooling rate exceeds the critical cooling rate, the martensitic transformation occurs which produces the highest strength and lowest ductility. In some sections that need a higher ductility, e.g. for the purpose of energy absorption during crash, a cooling rate lower than the critical one is used [2]. Füller [3] explored a concept for a partial hardening zone which is softer than the remainder of the part. The work indicated that the soft zone could be achieved by controlling the cooling rate lower than the critical cooling rate of a material. Bruschi et al. [4] and Mori et al. [5] showed that the control of the phase transformation through the thermal history in the workpiece during the forming and quenching is a very important factor in the design of the hot stamping process. The investigation of Rohde et al. [6] also showed that different phase fraction of ferrite, bainite and martensite are formed dependent on the thermal history of the workpieces. According to the study by Nikravesh et al. [7] the critical cooling rate increases from approximately 15°C/s to 60°C/s by inducing deformation. In case of ferrite and pearlite, it is reported that the deformation of austenite increases the density of ferrite nucleation sites due to the increase in austenite grain boundary surface and the higher density of dislocations, which raises the free energy of the austenite and leads to an increased driving force for the austenite-ferrite transformation. As a result, the fractions of ferrite and pearlite rise as plastic deformation is increased. The investigation from Bhadeshia [8] shows that the austenite deformation during the thermo-mechanical processing of steel accelerates also the rate of the bainitic reaction. Grains and subgrains, which are affected by the deformation, are suitable nucleation sites also for the bainitic transformation.

A first model of austenite decomposition for hot stamping has been implemented by Åkerström et al. [9]. In this model, the martensite transformation is described as diffusionless phase transformation according to the equation obtained from Koistinen et al. [10]. However, the disadvantage of this model is that it cannot accurately approximate the dependency on supercooling. To improve this, the rate based approach to the temperature introduced by Lee et al. [11] was implemented by Hippchen et al. [12]. Additionally, they extended the transformation equation by accounting for the effect of carbonization of the retained austenite by introducing a description of the saturation of formation of martensite in dependence on the amount of retained austenite at the martensite start temperature.

Ferrite, pearlite, and bainite transformations, which are diffusion-controlled phase transformation, can be modeled by the equation from Kirkaldy et al. [13]. According to [9], the hot stamping process is not a process with a continuous cooling rate. It is necessary to control the incubation time and the rate of decomposition in dependence of the cooling conditions. Therefore, they proposed the extrapolation of a material depend phase diagram from Hultgren et al. [14], and also introduced a grain boundary parameter and specific transformation kinetic parameters. The work from Muszka et al. [15] presented a microstructure-based numerical model including deformation and further process parameters. The aim of this study is to establish a model for the press-hardening steel 22MnB5, accounting for the effect of pre-strain on the transformation kinetics. The model uses dependencies of model parameters on the pre-strain and cooling rate, making use of the information contained in the experimental data. The experimental results are used to

calibrate and validate the material model. After the calibration, an attempt to predict the dilatation curves by interpolating data between two simulation points is made.

2. CHARACTERIZATION

Specimens of 22MnB5 steel with a thickness of 1.5 mm were manufactured for hot tensile testing. Metallographic analyses were carried out to characterize the as-delivered conditions. The steel consists of a ferritic-pearlitic microstructure with 72 vol. % (±5%) ferrite and 28 vol. % (±5%) pearlite.

2.1. HOT TENSILE TESTING

The hot tensile tests were performed on a quenching/deformation dilatometer DIL805A/D. The gauge length and width were 10 mm and 5 mm, respectively. The rolling direction coincides with the testing direction.

In the present investigation, the specimens were deformed to different strain levels with a strain rate of 1 s^{-1} and quenched down to the room temperature with a defined cooling rate. Tensile tests were conducted in vacuum of 10^{-4} mbar. Thermocouple type S was spot welded on the middle position of the gauge length to detect the temperature of the specimen surface.

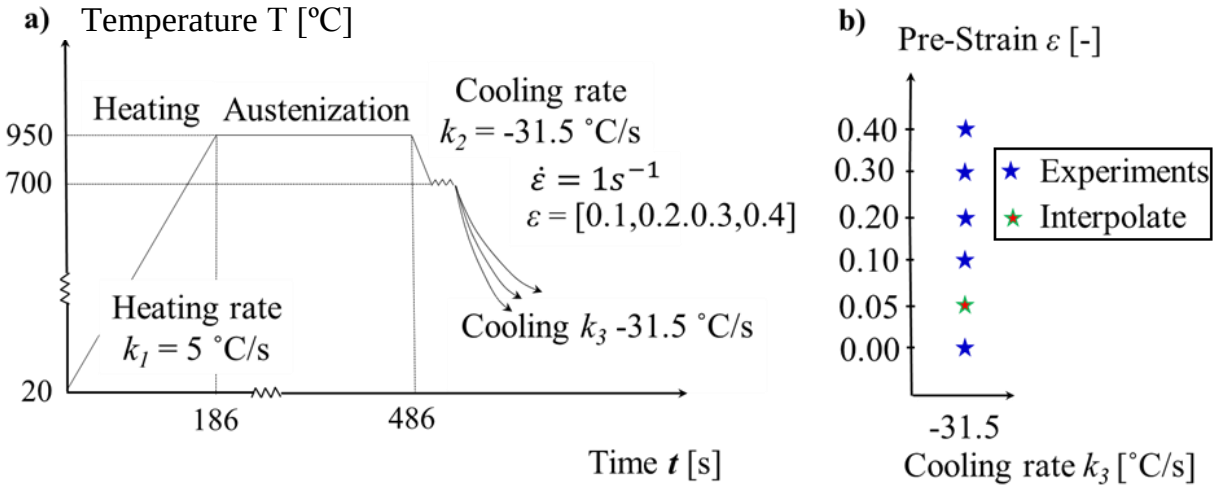

Fig. 1. a) Test conditions for model calibration and b) pre-strain for analyzing the interpolation with the obtained model

The specimens were heated with a heating rate of 5°C /s to the temperature of 950°C and held for 300 s to obtain a homogeneous microstructure. Then, the temperature was reduced to 700°C with a cooling rate of –31.5°C/s and the specimens were deformed isothermally under tension to the defined levels and quenched down with the cooling rate

–31.5°C /s to room temperature. The critical cooling rate of 22MnB5 is –27°C/s. In order to ensure the full martensite transformation, the cooling rate is increased from –27°C/s to –31.5°C/s. The different pre-strains are shown in Fig. 1b. Four tests are used for model calibration and one test with a pre-strain of 0.05, is used of prove the possibility of a linear interpolation with the simulation model.

2.2. EXPERIMENTAL RESULT

To evaluate the final microstructure, the specimens for making the microstructure investigation are cut from the gauge length where the uniform strain distribution can be obtained. The samples are then mounted, polished and later on etched with Beraha I agent to reveal the microstructure by using a light optical microscope (LOM). The final phase fraction of the specimens can be quantitatively evaluated by using the software Atlas. This software estimates the final phase fraction of the specimens by distinguishing the colour shades of pictures obtained from LOM. As shown in Fig. 2a, there are 3 main colours which can be observed in the picture captured by the LOM: black (martensite), brown (bainite), and white (Ferrite and retained austenite). The software distinguishes these colours, and qualitatively evaluates the phase fractions in the picture according a colour defined by a user. In this case the brown colour (bainte) will be replaced by the blue colour as shown in Fig. 3b. With these investigations, the quantitative phase fractions are determined for several pre-strains. The microstructure of the specimens after the tests is illustrated in Fig. 2c-2f.

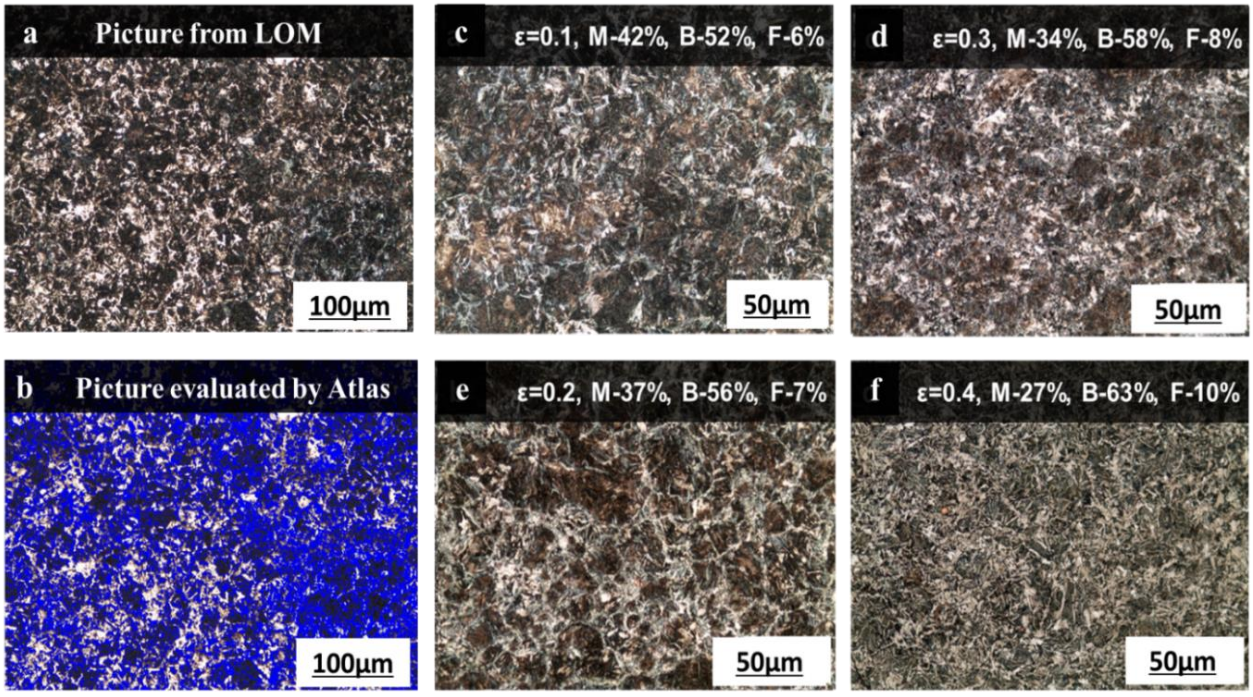

Fig. 2. a) Figure obtained from LOM, b) the quantitative microstructure evaluation by Atlas software, c)–f) microstructure at pre-strains from 0.1–0.4

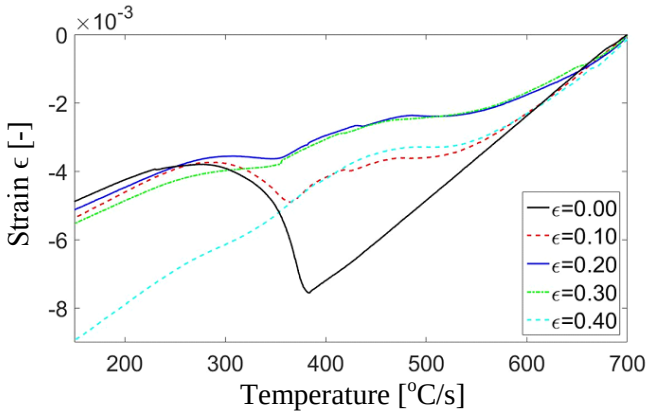

Fig. 3. Dilatation of from the experiment

Since the dilatometer provides the dilation curves after testing, the dilations from each test are converted into strain values and plotted over the temperature as shown in Fig. 3. Without deformation, it can clearly be seen that the specimen undergoes a martensitic transformation without signs of ferrite or bainite transformation. When the pre-strain is applied at the same cooling rate, bainite starts to form. As the deformation increases, more bainite and ferrite forms and less martensite can be observed from the microstructural evaluation.

3. MODELLING OF HOT STAMPING SIMULATION

The simulation of the phase transformation is implemented using the simulation software LS-Dyna. The boundary conditions of the simulation are set up according to the experiment. The material law number 248 (MAT 248) is employed in order to observe the forming and phase transformation behaviours of the material.

Martensite Phase Evolution

$$\frac{d\xi_m}{dT} = \alpha_m (M_S - T)^n \xi_m^{\varphi_m} (1-\xi_m)^{\psi_m{}^{(2-\xi_a)}}$$

Kinetics for Ferrite, Pearlite and Bainite

$$\frac{d\xi_f}{dt} = 2^{\omega_f G} \frac{exp\left(-\frac{Q_f}{RT}\right)}{C_f} (F_S - T)^3 \frac{\xi^{\varphi_f{}^{(1-\xi_f)}} (1-\xi_f)^{\psi_f \xi_f}}{exp(C_{r,f}\xi_f^2)}$$

$$\frac{d\xi_p}{dt} = 2^{\omega_p G} \frac{exp\left(-\frac{Q_p}{RT}\right)}{C_p} (P_S - T)^3 \frac{\xi^{\varphi_p{}^{(1-\xi_p)}} (1-\xi_p)^{\psi_p \xi_p}}{exp(C_{r,p}\xi_p^2)}$$

$$\frac{d\xi_b}{dt} = 2^{\omega_b G} \frac{exp\left(-\frac{Q_b}{RT}\right)}{C_b} (B_S - T)^3 \frac{\xi^{\varphi_b{}^{(1-\xi_b)}} (1-\xi_b)^{\psi_b \xi_b}}{exp(C_{r,b}\xi_b^2)}$$

Start Temperatures

$$F_S = 273.15 + 912 - 203 \cdot \sqrt{C} - 15.2 \cdot Ni + 44.7 \cdot Si + 104 \cdot V + 31.5 \cdot Mo + 13.1 \cdot W - 30 \cdot Mn - 11 \cdot Cr - 20 \cdot Cu + 700 \cdot P + 400 \cdot Al + 120 \cdot As + 400$$

$$P_S = 273.15 + 723 - 10.7 \cdot Mn - 16.9 \cdot Ni + 29 \cdot Si + 16.9 \cdot Cr + 290 \cdot As + 6.4 \cdot W$$

$$B_S = 273.15 + 637 - 58 \cdot C - 35 \cdot Mn - 15 \cdot Ni - 34 \cdot Cr - 41 \cdot Mo$$

$$M_S = 273.15 + 539 - 423 \cdot C - 30.4 \cdot Mn - 17.7 \cdot Ni - 12.1 \cdot Cr - 7.5 \cdot Mo + 10 \cdot Co - 7.5 \cdot Si$$

Fig. 4. Main model equations

In this model, the phase transformation from austenite to ferrite, pearlite, and bainite can be modeled as diffusion controlled phase transformations, and for the phase transformation from austenite to martensite, the model employs a diffusionless phase transformation model. The equations of the model are summarized in Fig. 4 and can be found in full detail in [16]. During the phase transformation, a volumetric expansion takes place due to the difference of packing density between the parent and child phase.

The volumetric change ($d\varepsilon_v$) has been implemented in the model using the following equation [12]

$$d\varepsilon_v = \frac{-1}{3(\rho + d\rho)} \sum_{i=1}^{n} d\zeta_i \rho_i \delta_{mn} \quad | \quad i = \gamma, f, p, b, m \tag{1}$$

where: δ_{mn} is the Kronecker Delta, ζ_i is the influence of the phase change in each time step, $(\rho + d\rho)$ is the final density, ρ_i is the phase specific density, and γ, f, p, b, and m denote austenite, ferrite, pearlite, bainite, and martensite respectively.

In order to include the effect of plastic deformation on the phase transformation in the model activation energy functions were introduced in prior work, cf. Bambach et al. [17], cf. Fig. 5. The activation energies thus replace the constant values originally foreseen in the model. In the present work, additional experiments are performed and the model is extended by making further model parameters dependent on pre-strain. The model is validated with conditions that were not used for model calibration.

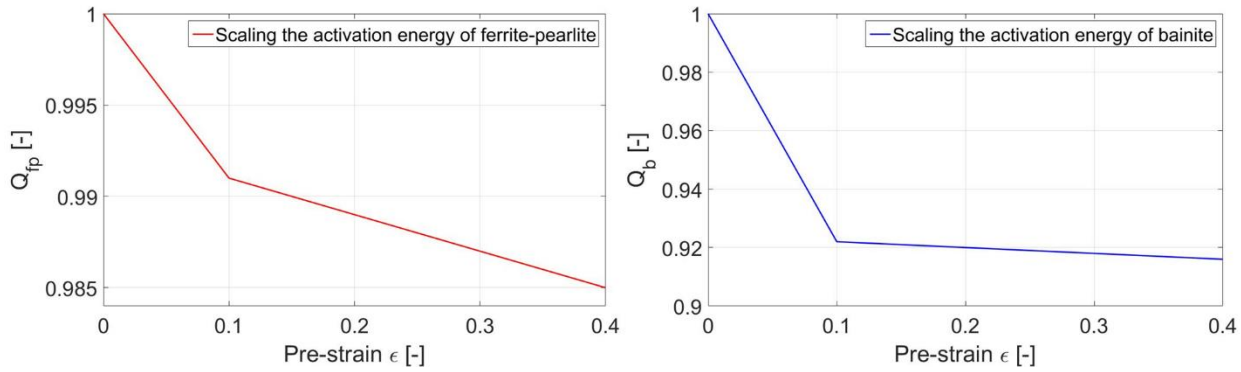

Fig. 5. Scaling of the activation energies for ferrite-perlite and bainite formation as a function of pre-strain

4. EVALUATION OF ACCURACY OF THE SIMULATION

The dilatation curves and predicted final microstructure are extracted from the simulation in order to compare them with those from the experiment as demonstrated in Fig. 6. The dilatation in the simulation is obtained by measuring the distance between the two nodes from the shoulders of the specimens. In the experiment, the dilatation of the specimens during the cooling results from 1) the thermal strain as a result of thermal contraction, and 2) the transformation-induced strain as the phase transformation starts.

This phenomenon originates from the difference of the packing density between the parent and product phases.

In order to match the curve between the simulation and experiment, the activation energy as well as the coefficients of thermal expansion (CTE) of austenite, bainite, and martensite, and the density difference between the parent and product phases are adjusted. The comparison between simulation and experiment under all test conditions is shown in Fig. 6a-6e.

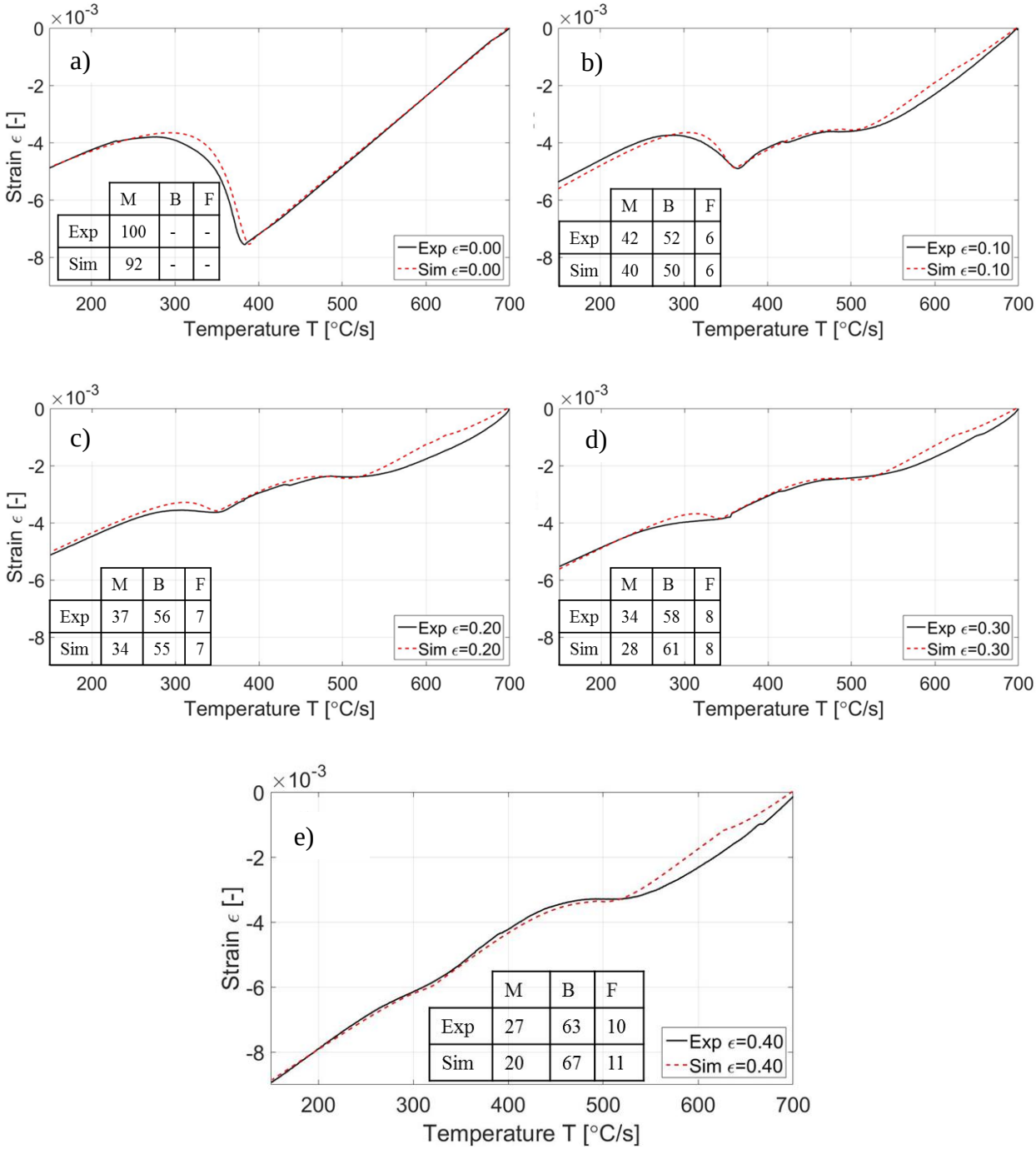

Fig. 6. Comparison between simulation and experiment

The result from the comparison indicates that the simulation follows the dilations obtained from the experiment fairly well. However, there are two regions that show some discrepancy. The first is the region from the starting temperature of quenching (700°C) until the bainite start temperature. The results from the simulation of this region are numerically calculated based on a linear thermal expansion coefficient, which leads to a linear contraction of the specimen. However, the dilatation curves extracted from the experiments do not behave in this manner. They tend to become non-linear as deformation is applied. Another region with discrepancies between model and experiment is the martensite transformation. The result indicates that the transformation in the experiment requires a longer time to finish than in the simulation.

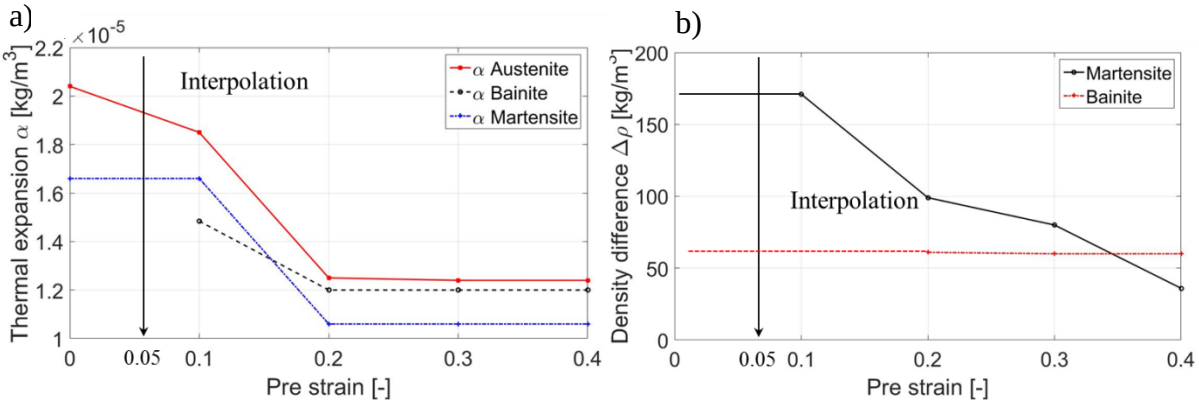

Fig. 7. Effect of pre-strain on the a) coefficient of thermal expansion and b) density difference

As the deformation increases from 0.1 to 0.2, the CTE of all phases significantly decreases until reaching constant values. When considering the density difference, it can be clearly seen that the pre-strain results in a reduction of the density difference between martensite and austenite. For the density difference between bainite and austenite, this effect cannot be observed.

5. INTERPOLATION BETWEEN RESULTS

The rise of deformation tends to increase the amount of ferrite, and bainite, and to decrease the CTE of all phases as well as the density difference between parent and product phases. This validity of this assumption will be checked by determining results between each test point by interpolation. Thus, a linear interpolation between the result at 0.0 and 0.1 was made to approximate the coefficients at a pre-strain 0.05. The reason for the interpolation between 0.0 and 0.1 that most of the hot stamping parts produced in the automotive industry do not undergo a large deformation. The interpolation values can be seen in Fig. 7. The CTE for austenite and martensite can be interpolated directly from the curves. For bainite, the same value as for the pre-strain of 0.1 is used because the bainite

starts to form at a pre-strain of 0.1. In order to obtain the value for the density difference of martensite the value at the pre-strain 0.1 used. Since the bainite does not show any change in density, a constant value is used. The comparison between the experiment and the interpolation result is illustrated in Fig. 8.

The result from the comparison reveals that the amount of dilatation due to the phase transformation of bainite and martensite is relatively well predicted. However, the interpolation result seems to predict a higher value of the CTE, causing a difference to the experiment.

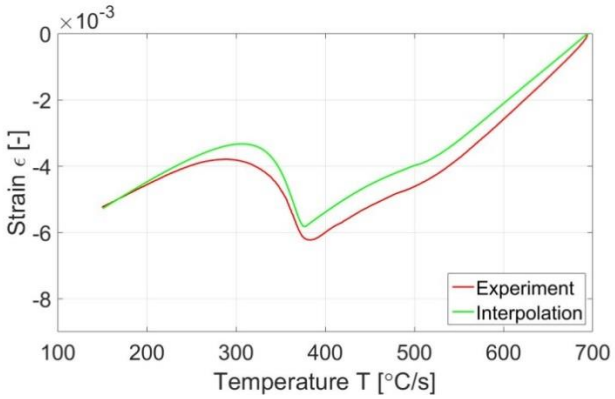

Fig. 8. Comparison between interpolation and the experiment

6. DISCUSSION

The investigation in this study shows that the CTE and the density of austenite changes as a function of the pre-strain. The CTE of any poly-crystalline metal or alloy is defined by the thermal expansion of the crystal and the texture. There are two possible effects of deformation on the CTE. The first is a change in the orientation of the crystals. The second is the partitioning of carbon between the phases during the phase transformation. The investigation from [18] indicated that the change in CTE is attributed to the change in orientation of crystal and also due to closure/opening of micro-cracks. They also found that the loading direction significantly changes the CTE. In compressing specimens, the CTE of thermal expansion was increased. On the other hand, the CTE decreased as a tensile loading was applied. This effect can be clearly seen from the simulation result. The CTE decreased as a function of pre-strain. In case of the carbon partitioning, it is reported in Ref. [19] that the CTE reduces as the carbon content increases.

The transformation-induced strain during phase transformation from austenite to martensite is due to the difference between the volumes between the austenite face-centered cubic (FCC) and the martensite body-centered tetragonal (BCT) structure. In the other words, the transformation-induced strain originates from the difference between the densities of each phase. The density difference is another parameter that has been adjusted during calibration of the model. It is adjusted to match the amount of the transformation-induced strain. There are possibly two reasons for the density difference in this study. Firstly, the work conducted by Loyer et al. [20] showed a change in density after tensile testing occurred. They suggested that the deformation caused a decrease

in density which is partly due to dislocations but mainly a consequence of the vacancies created by dragging of jogs in dislocations. Another possibility is described in Ref. [21].

The phase transformation from austenite to bainite depletes the amount of carbon in austenite. In the experiments, bainite is formed at temperatures around 500°C which is the range of the upper bainite phase transformation (550-400°C). In steel with a high carbon content, the transformation begins with the diffusion-controlled precipitation of cementite. As a result, the amount of carbon in austenite is significantly reduced. The lack of carbon in austenite results in a reduction in the relative change in volume during the martensite transformation. This makes the magnitude of the transformation-induced strain reduce when the deformation is increased.

7. CONCLUSION

The result from the experiments indicates that the deformation during the austenite significantly affects the transformations and hence the final properties of the material. As the pre-strain is increased, more bainite is formed. The effect can be included in the simulation by introducing a scaled activation energy function which represents the reduction of the activation energy as a function of pre-strain. After calibrating the model, some of the material parameters, in this case, CTE and the density of austenite, bainite, and martensite were also defined as function of pre-strain. It is found that the CTE and the density of austenite tend to decrease as the pre-strain increases. The plot of the reduction of CTE and the density change made it possible to predict the resulting parameter values within the experimental range by linear interpolation. An attempt to predict the dilatation at the pre-strain of 0.05 was made by interpolating the result between the pre-strains 0.0 and 0.1. The result shows that the simulation follows the experimental curves well but also shows some differences. The interpolation seems to predict lower CTE values for the austenite. However, the amount of the phase transformation induced by the pre-strain matches well. The results show that it appears to be possible to extend a given model by accounting for the dependence of model parameters on testing conditions. Using sufficient experimental data could pave the way to make existing models more accurate.

ACKNOWLEDGEMENTS

The authors would like to thank the BTU Cottbus-Senftenberg for supporting this research within the graduate research school (GRS) "LocPro".

REFERENCES

[1] KARBASIAN H., TEKKAYA A.E., 2010, *A review on hot stamping*, Journal of Materials Processing Technology, 210/15, 2103–2188.

[2] PAUL A., REUTHER F., NERMANN F., ALBERT A., LANDGREBE D., 2017, *Process simulation and experimental validation of hot metal gas forming with new press hardening steel*, Journal of Physics, Conf. Series 896.

[3] FÜLLER K.-H., 2010, *Leichtbau-Konzepte, Werkstoffe, Produktionstechnologien*, In: CHIMANI C.M., FRAGNER W., UGGOWITZER P.J., WAHLEN A. (Hrsg), 6, Ranshofener Leichtmetalltage, Ranshofern, Munderfing, Aumayer Druck und Verlags GmbH. & Co KG, 163–173.
[4] BRUSCHI S., GHIOTTI A., 2014, *Hot stamping, In comprehensive materials processing*, edited by HASHMI S., BATAIHA G.F., TYNE C.J.V., YILBAS B., Elsevier, Oxford, 27–54.
[5] MORI K.Y., BARIANI P.F., BROSIUS A., BRUSCHI S., MAENOE T., MERKLEIN M., YANAGIMOTO J., 2017, *Hot stamping of ultra-high strength steel parts*, CIRP Annals, 66/2, 755–777.
[6] ROHDE J., JEPPSSON A., 2000, *Literature review of heat treatment simulation with respect to phase transformation, residual stresses, and distortion*, Scandinavian Journal of Metallurgy. 29, 47–62.
[7] NIKRAVESH M., NADERI M., AKBARI G.H., BLECK W., 2015, *Phase Transformation in a simulated hot stamping process of boron-bearing steel*, Material and Design, 84, 18–24.
[8] BHADESHIA H.K.D.H., 2001, *Bainite in Steels, Transformations, Microstructure and Properties*, 2nd ed. IOM Communications Ltd, Cambridge, 203–213.
[9] ÅKERSTRÖM P., OLDENBURG M., 2006, *Austenite decomposition during press hardening of a boron steel-Computer simulation and test*, Journal of Materials Processing Technology, 174/1–3, 399–406.
[10] KOISTINEN D.P., MARBURGER R.E., 1959, *A general equation prescribing the extent of the austenite-martensite transformation in pure iron-carbon alloys and plain carbon steels*, Acta Metallurgica, 7, 59–60.
[11] LEE S.J., PAVILINA E.J., VAN TYNE C.J., 2010, *Kinetics modelling of austenite decomposition for an end-quenched 1045 steel*, Mater. Sci Eng. A, 527, 3186–3194.
[12] HIPPCHEN P., LIPP A., GRASS H., CRAIGHERO P., FLEISCHER M., MERKLEIN M., 2016, *Modelling kinetics of phase transformation for the indirect hot stamping process to focus on car body parts with tailored properties*, Journal of Material Processing Technology, 228, 59–67.
[13] KIRKALDY J.S., VENUGOPALAN D., 1983, *Prediction of microstructure and hardenability in low-alloy steels*, Phase Transformation in Ferrous Alloys, 125–148.
[14] ULTGREN A., 1938, *Diskussion über "The Physics of Hardenability"* von R.F. Mehl. Hardenability of Alloy Steels, 55–56.
[15] MUSZKA K., MADEJ L., STEFANSKA-KADZIELA M., MAJTA J., 2014, *Microstructure-based numerical modelling of manufacturing processes of nanolayered material*, Journal of Machine Engineering, 14/1, 39–52.
[16] Material Model, 2015, *Ls-Dyna keyword user's manual,* 2, Livermore Software Technology Corporation.
[17] BAMBACH M., BUHL J., HART-RAWUNG T., LECHNER M., MERKLEIN M., *Towards virtual deformation dilatometry for design of hot stamping process*, Procedia Engineering, (in print).
[18] YAFEI S., YONGJUN T., JING S., DONGJIE N., 2009, *Effect of temperature and composition on thermal properties of carbon steel*, CCDC 2009, Chinese Control and Decision Conference.
[19] PRESTON S.D., MARSDEN B.J., 2005, *Changes in the coefficient of thermal expansion in stressed Gilsocarbon graphite*, Carbon 44, 1250–1257.
[20] LOYER A., DORLOT J.M., 1970, *Density change in Iron after tensile test*, Phys. Stat. Sol. (a) 2, 91.
[21] BLECK W., 2013, *Material science of steel*, Department of Ferrous Metallurgy, RWTH Aachen University.